

Article

# Examination of Chaotic Structures in Semiconductor or Alloy Voltage Time-Series: A Complex Network Approach for the Case of TlInTe<sub>2</sub>

Dimitrios Tsiotas <sup>1,2,3,\*</sup> , Lykourgos Magafas <sup>3</sup>  and Michael P. Haniias <sup>3</sup>

<sup>1</sup> Department of Regional and Economic Development, Agricultural University of Athens, Nea Poli, 33100 Amfissa, Greece

<sup>2</sup> School of Social Sciences, Hellenic Open University, 10677 Athens, Greece

<sup>3</sup> Laboratory of Complex Systems, Department of Physics, International Hellenic University, Kavala Campus, 65404 St. Loukas, Greece; lmagafas@otenet.gr (L.M.); mhaniias@physics.ihu.gr (M.P.H.)

\* Correspondence: tsiotas@aua.gr

Received: 2 October 2020; Accepted: 13 November 2020; Published: 20 November 2020



**Abstract:** This paper proposes a method for examining chaotic structures in semiconductor or alloy voltage oscillation time-series, and focuses on the case of the TlInTe<sub>2</sub> semiconductor. The available voltage time-series are characterized by instabilities in negative differential resistance in the current–voltage characteristic region, and are primarily chaotic in nature. The analysis uses a complex network analysis of the time-series and applies the visibility graph algorithm to transform the available time-series into a graph so that the topological properties of the graph can be studied instead of the source time-series. The results reveal a hybrid lattice-like configuration and a major hierarchical structure corresponding to scale-free characteristics in the topology of the visibility graph, which is in accordance with the default hybrid chaotic and semi-periodic structure of the time-series. A novel conceptualization of community detection based on modularity optimization is applied to the available time-series and reveals two major communities that are able to be related to the pair-wise attractor of the voltage oscillations' phase portrait of the TlInTe<sub>2</sub> time-series. Additionally, the network analysis reveals which network measures are more able to preserve the chaotic properties of the source time-series. This analysis reveals metric information that is able to supplement the qualitative phase-space information. Overall, this paper proposes a complex network analysis of the time-series as a method for dealing with the complexity of semiconductor and alloy physics.

**Keywords:** voltage oscillations; complex network analysis of time-series; community detection; chaotic time-series

## 1. Introduction

Semiconductors are materials with temperature-dependent electrical conductivity, with conductivities ranging between those of conductors (e.g., Cu) and those of insulators (e.g., SiO<sub>2</sub>) [1–3]. This characteristic property is the result of their incomplete (doped) crystal structure, which generally causes a decrease in their resistivity (and thus an increase in their conductivity) with an increase in temperature, in contrast to the typical behavior of metals [4]. Semiconductors have a range of useful properties, such as facilitating the transit of current in one direction rather than in the other, providing differential resistance, and exhibiting sensitivity to light or heat [3]. Given that their electrical properties are dependent either on doping or on the effect of electrical fields or light, semiconductor devices are widely used for applications such as amplification, switching and energy conversion, and have led to the development of transistors, integrated circuits, radio receivers, and many other communication devices [2,3]. Research in the field of semiconductors is, by definition, characterized

by high levels of complexity due to their deviation from typical crystal structures that causes their temperature-dependent conductivity [5]. Therefore, the modern conceptualization and understanding of semiconductor properties builds on quantum physics and other fields of complexity science to explain the nonlinear charge-carrier behavior within crystal lattice structures [3,5]. The relationship between voltage and current in metallic conductors is linear, and the same is true for semiconductors with low current or voltage values. At higher values, though, this relationship becomes nonlinear. A special case appears when the phenomenon of negative differential resistance (NDR), in which voltage decreases as the current increases, appears in the linear region. When this change is abrupt, the switching effect takes place [6–8].

For instance, the ternary (i.e., consisting of three different elements) semiconductor  $TLMX_2$  [8], with  $M=Ga$  (Gallium) and  $In$  (Indium), and  $X=Se$  (Selenium),  $S$  (Sulfur) and  $Te$  (Tellurium), as well as the  $TlInX_2-TLSmX_2$  alloys [9], with  $X=S, Se, \text{ or } Te$ , exhibit nonlinear effects on their current-voltage ( $I-V$ ) characteristics (including a region of negative differential resistance), switching, and memory effects [6–8]. The electrical conductivity of several chain-type crystals exhibits time oscillations and intermittency [6–8,10]. These nonlinear effects, such as negative differential resistance, are the result of an electro-thermal mechanism [6,7,10]. The switching occurs because of deviations in the uniform distribution of the imperfection. Chain-type structures permit the generation of high current density filaments that act as channels between the two electrodes. Because of Joule heating, two parallel resistors exist—one high and one low. The high current density leads to Joule heating, and because of Joule heating the resistor becomes smaller. This process produces an S-type  $I-V$  characteristic [6,7,10]. Due to the instabilities in carrier diffusion and recombination, chaotic oscillations occur [6,7].

Within this context, nonlinear conceptualizations in research related to semiconductors have been evident in the literature for almost three decades [1,3,4], with respect to aspects such as structure [2], dynamics [2,11,12], optical behavior [11,13], energy applications [14], and physical properties [2,15]. Indicatively, the characteristic approaches in semiconductor research are built on nonlinear stochastic processes [11], quantum physics modeling of conductivity in semiconductors [3,5], nonlinear and chaotic time-series analysis [5–7,13], and the structural modeling of super-lattice topologies [12]. Among such approaches, there are a couple of works that use the network paradigm to deal with the issues of complexity that govern either structural or functional connectivity in semiconductors, such as the work of [16], who introduced the application of queuing network models for the design and analysis of semiconductor wafer fabs, and the more recent work of [17], who applied complex network analysis to study cluster synchronization in mutually coupled semiconductor laser (SLs) networks with complex topologies. Although these examples are obviously not enough to support, epistemologically, the contribution of network science [18,19] to the established field of semiconductor research, they appear to have the merit of highlighting the potential linkage between these two research fields that is defined by their common area, that is, dealing with complex systems and complexity in general.

Network science is a modern discipline, using the network paradigm to model communication systems into pair-sets of nodes and links, and it has been proven as a fruitful field of interdisciplinary research, providing insights into the structure and functionality of complex interconnected systems [18,19]. For instance, the contribution of network science to time-series analysis has led to the research field of “complex network analysis of time-series”, which enjoys several applications in various disciplines and fields of science [20]. This research field deals with methods for transforming a time-series into complex networks, which allows for managing a time-series with a higher complexity level by studying the topological properties of graphs instead of the time-series’ structural properties [21–25]. A major contribution in this research field was made by [24], who proposed an algorithm, named the natural visibility graph algorithm (NVG), based on an optics criterion for transforming a time-series into a graph. The authors showed that their algorithm was sufficient to convert fractal series into scale-free networks, supporting the fact that power-law degree distributions are related to fractality [24]. Some indicative applications of the complex network analysis of time-series

include the work of [26], who observed that the scale-free property in visibility graphs associated to the time-series of energy dissipation rates corresponds to the self-similarity of the energy dissipation rate series and, also, that the hub-to-hub attraction, which was detected in the network, explains the absence of self-similarity in the series. In the work of [27], which was conducted on an experimental temperature time-series set extracted from a vertical turbulent jet, the authors observed that the complex network approach allows a more detailed detection of various dynamical regions of the jet-flow in a time-series, which was constructed from a vertical turbulent heated jet. In the work of [28], the authors observed that the average clustering coefficient of a limited penetrable horizontal visibility graph, which was created from oil–water two-phase flow signals, allows the identification of the typical oil–water flow patterns at different scales. Furthermore, the authors of [29] showed that the power averaging aggregation operator, which is computed on the associated visibility graph, is more effective than other time-series operators. In the work of [30], the authors observed that the visibility graph-based approach unveils the key temporal properties of the turbulent time-series and their changes due to positive vertical coordinate movements. In the work of [31], the authors applied the NVG to convert the prime Greek COVID-19 infection curve into a graph. By using the modularity optimization algorithm, they divided the associated visibility graph into connected communities, which revealed within the time-series body a sequence of different typologies introducing the saturation stage in the evolution of the pandemic, a fact that was verified by the global maximum appearing at the beginning of the saturation stage in terms of Gaussian modeling, and by following observations.

Within the context of converting a time-series into a visibility graph, the graph model associated to the time-series appears to inherit structural properties that are consistent with the fractal-like and self-similarity characteristics of the source time-series [24,26] and it can generally include immanent structural information that is related to the configuration of the physical system it represents [28–31]. Within this framework, this paper studies the chaotic oscillations and the corresponding phase portrait of an already known semiconductor's time-series by using the complex network analysis of time-series. This study can also apply to alloys that exhibit the same non-linear behavior, or their electrical properties. The analysis aims to examine the structural properties that are immanent in the graph structure associated to the time-series, and to compare the complex network approach with the already known results of the chaos detection analysis of the time-series. The further purpose of the paper is to address the demand for managing the complexity of semiconductor research, with the interdisciplinary approach of complex network analysis of time-series being already effective in various applications.

The remainder of this paper is organized as follows: Section 2 describes the methodology and data of the study, building on the natural visibility algorithm that is introduced by [24] and on the previous study [7] for detecting quasi-periodic and chaotic self-excited voltage oscillations in a ternary semiconductor. Section 3 shows the results of the analysis and discusses them in comparison with the available findings of the previous work, and, finally, in Section 4, conclusions are given.

## 2. Data and Methodology

The methodological framework of the study builds on the complex network analysis of time-series to transform into a complex network a time-series of voltage oscillations recorded in a ternary semiconductor, as was previously studied by the authors of [7], so that to study the topology of the associated graph instead of the time-series. The algorithm applied for the transformation of the time-series into a graph is the natural visibility algorithm (NVGA) proposed by [24] and it is described in detailed in the following. The overall analysis is implemented in three discrete steps; first, the source time-series is transformed into a graph model by using the NVGA. At the second step, the topological properties of the associated visibility graph are studied, and the secondary time-series are created by projecting major network node measures of the visibility graph onto the time-series' body. At the final step, the associated visibility graph is divided into connected communities, and correspondences to the source time-series are applied to extract structural information about the

time-series in terms of connectivity. Each step of the methodological framework is described in more detail in the following paragraphs.

### 2.1. Data

The available time-series dataset was extracted from the work of [7] and represents typical voltage oscillations of the ternary semiconductor  $\text{TlInTe}_2$  (i.e., thallium indium ditelluride single crystal), as monitored in the negative differential resistance (NDR) region of a representative  $I$ - $V$  characteristic curve, shown in Figure 1, at an ambient temperature of 77 K and for a fixed current value of  $I = 1.15$  mA.

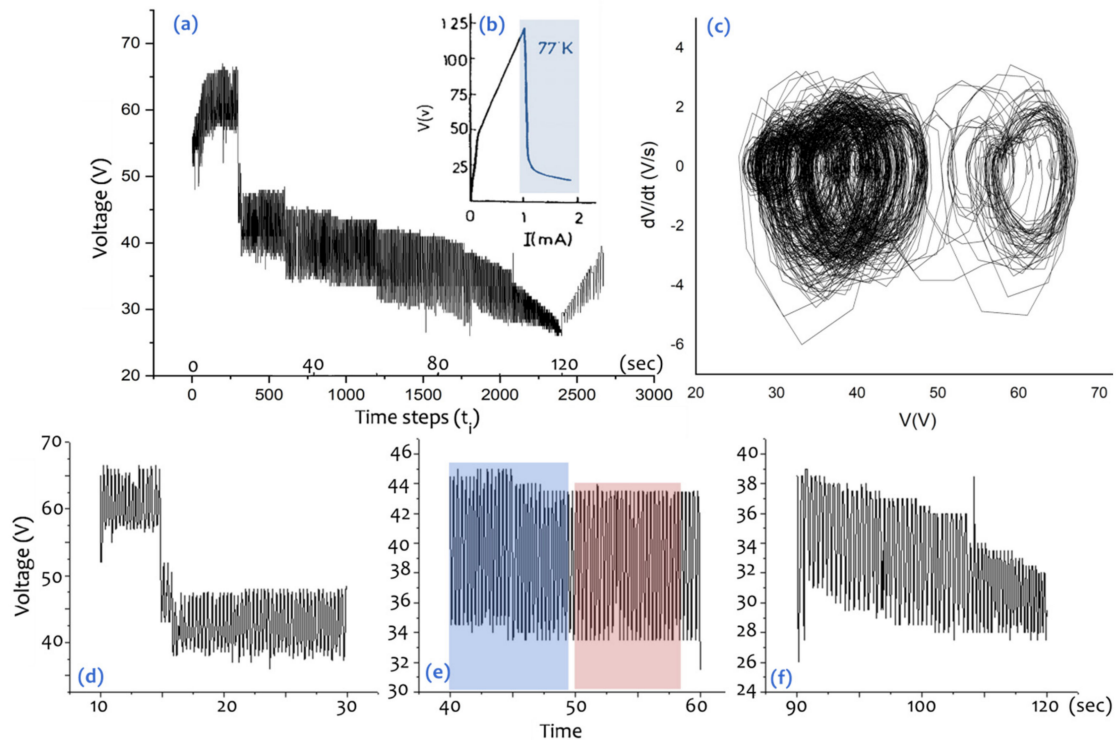


**Figure 1.** (a) The available time-series expressing typical voltage oscillations as monitored in the negative-differential-resistance (NDR) region of (b) a representative current-voltage ( $I$ - $V$ ) characteristic as registered on  $\text{TlInTe}_2$ , at an ambient temperature 77 K and for a fixed current value  $I = 1.15$  mA (marked by the blue area), (c) The phase portrait of voltage oscillations, (d) part of chaotic oscillations in the time-series, (e) a semi-periodic section in the NDR region, ranging from 40 to 49 s (blue area), and a periodic one, ranging from time  $t = 50$  s to  $t = 57$  s (red area), (f) part of chaotic oscillations in the time-series (source: [7]).

The available dataset of the time-series is invariant to repetitions to the extent that any repetition of the experiment applied under the same experimental conditions (i.e., temperature and current values) can lead to the same time-series structure [7], which is shown in Figure 1. In particular, the existence of chaotic oscillations of current or voltage in the region of NDR semiconductors can be considered as completely repeatable since, due to the chaotic nature of the phenomenon, small changes in the initial experimental conditions may generate different but always chaotic oscillations, which will have the same invariant parameters [7]. Within this context, this paper uses such chaotic voltage oscillations data in the NDR to apply complex network analyses to time-series, to contribute to the understanding of this phenomenon. The available time-series consists of  $n = 2672$  nodes (time-steps with sample rate  $\Delta t = 0.05$  s) [7]. The voltage oscillation in the time-series ranges within the interval [26 V, 67 V]. Voltage oscillations are produced by an intermittency mechanism, which implies that for some current values, the oscillations are periodic, semi-periodic, and chaotic. When oscillations are chaotic, for the given current value, there are possible areas where the oscillations can be quasi periodic.

For instance, Figure 1e shows a periodic section, ranging from  $t = 50$  s to  $t = 57$  s, and a semi-periodic one, ranging from 40 to 49 s. Chaotic oscillations are also shown in Figure 1c,f, respectively [7]. The form of the phase-space of the available time-series has a characteristic non-periodic nature, which is consistent with the behavior of the non-periodic trajectories in the phase portrait that is shown in Figure 1c. These trajectories appear to lie within the basin of a seemingly uniform attractor. Qualitatively, the phase portrait of the available time-series is considered as the projection of a strange attractor [7].

### 2.2. Complex Network Analysis of Time-Series: The Natural Visibility Graph Algorithm

The analysis aims at studying the effects of the NDR state, which are mainly chaotic oscillations. In most cases, the chaotic voltage oscillations in the NDR region are due to an electrothermal mechanism or to a pure electronic mechanism. In particular, in the case of TlInTe<sub>2</sub>, the NDR is due to an electrothermal mechanism [6]. Provided that the main goal is to understand the underlying mechanism of such chaotic oscillations, and in order to distinguish between these two specific processes, we apply a complex network analysis of time-series, which has become rather effective in the analyses of time-series of fractal-like and self-similar structures [24,26]. As far as the authors know, this approach is here applied for the first time to this kind of material, and is expected to reveal information about the transport phenomena, which in the case of this study regard the current filaments and their connections, and thus to enhance the existence of an electrothermal mechanism. The natural visibility algorithm (NVGA) was proposed by the authors of [24] and conceptualizes a time-series as a landscape [32,33]. In particular, the NVGA considers a time-series as a chain of successive mountains of different heights, whereby an observer standing on each node (time-point) can see in both directions for as far as there is no other node obstructing its visibility (Figure 2).

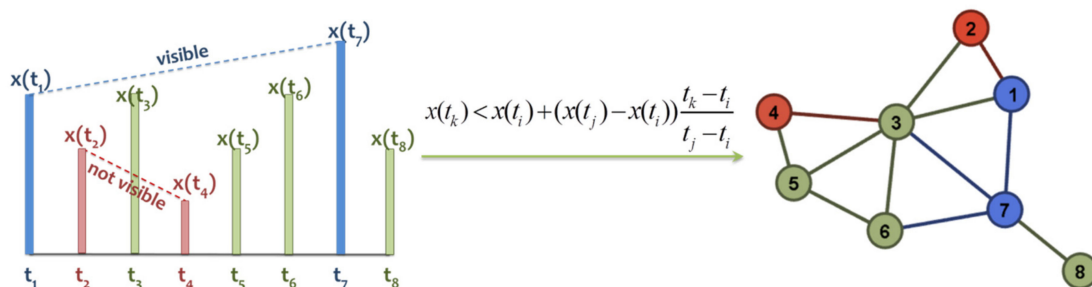


**Figure 2.** (left) Example of a pair of visible (in blue) and not visible (in red) time-series nodes according to the natural visibility algorithm (NVG); (right) the visibility graph associated to the time-series shown at the left side.

In mathematical terms, each ordered node  $(t_k, x(t_k))$  in the time-series, where  $x(t_k)$  denotes the numerical values of the time-series nodes at time  $t_k$ , corresponds to a graph node  $n_k \equiv (t_k, x(t_k)) \in V$ . In the associated visibility graph  $G(V,E)$ , with  $V$  expressing the node-set and  $E$  the edge-set, a pair of nodes  $n_i, n_j \in V$  is connected  $(n_i, n_j) \in E$  when the following NVG connectivity criterion (inequality) are satisfied by the intermediate nodes  $n_k$  [24]:

$$x(t_k) < x(t_i) + (x(t_j) - x(t_i)) \frac{t_k - t_i}{t_j - t_i}, \tag{1}$$

where  $n_i \equiv (t_i, x(t_i))$  expresses the graph nodes and  $(t_j, x(t_j))$  their corresponding time-series nodes. In geometric terms, a visibility line can be drawn between two time-series nodes,  $(t_i, x(t_i))$  and  $(t_j, x(t_j))$ , if no other intermediating node  $(t_k, x(t_k))$  obstructs their visibility. This implies that no other node intermediating the pair  $(t_i, x(t_i))$  and  $(t_j, x(t_j))$  is higher and can intersect the visibility line created by nodes  $(t_i, x(t_i))$  and  $(t_j, x(t_j))$ , as is shown in Figure 2. Therefore, two nodes  $n_i \equiv (t_i, x(t_i))$  and  $n_j \equiv (t_j, x(t_j))$  in the time-series can enjoy a connection  $(n_i, n_j) \in E$  in the associated visibility graph  $G(V,E)$  when they

are visible via a visibility line. The visibility algorithm interprets the time-series as a landscape and generates a visibility graph illustrating this landscape in terms of complex network representation, wherein complex network analysis can be further applied [24,32,33].

### 2.3. Network Analysis

The visibility graph is an undirected and unweighted graph model [32,33], wherein network analysis can be applied to examine its topology and hierarchical structure. The network measures used for the analysis of the visibility graph are shown in Table 1, and they were extracted from the sources [34–36].

**Table 1.** Network measures (\*) used in the analysis.

Measure	Symbol	Description	Math Formula
Graph density	$\rho$	The fraction of the existing connections of the graph ( $m$ ) to the number of the possible connections (equal to $\binom{n}{2}$ , where $n$ is the number of nodes). It expresses the probability to meet in the GMN a connected pair of nodes.	$\rho = m / \binom{n}{2} = \frac{2m}{n \cdot (n - 1)}$
Node Degree	$k$	The number of edges $k(i)$ being adjacent to a given node $i$ belonging to a graph $G(V,E)$ , where $V$ is the node-set and $E$ is the edge-set. Node-degree expresses the node’s communication potential.	$k_i = k(i) = \sum_{j \in V} \delta_{ij}$ , where $\delta_{ij} = \begin{cases} 1, & \text{if } e_{ij} \in E \\ 0, & \text{otherwise} \end{cases}$
Node strength	$s$	For a network edge $e_{ij} \in E$ , where $E$ is the edge-set, the node-strength $s(i)$ is defined by the sum of edge weights $w_{ij}$ being adjacent to a given node $i$ .	$s_i = s(i) = \sum_{j \in V} \delta_{ij} \cdot w_{ij}$
Average Path Length	$\langle l \rangle$	The average length of the network shortest-paths $d(i,j)$ , where $n$ is the number of nodes in the network.	$\langle l \rangle = \frac{\sum_{i \in V} d(i, j)}{n \cdot (n - 1)}$
Clustering Coefficient (local)	$C(i)$	The probability of meeting linked neighbors around a node $i$ , which is equivalent to the number of the node’s connected neighbors $E(i)$ (i.e., the number of triangles that are configured in the neighborhood), divided by the number of the total triplets shaped by this node, which equals to $k_i(k_i-1)$ , where $k_i$ is the degree of node $i$ .	$C(i) = \frac{E(i)}{k_i \cdot (k_i - 1)}$
Modularity	$Q$	An objective function expressing the potential of a network to be subdivided into communities. In its mathematical formula, $g_i$ is the community of node $i \in V$ (where $V$ is the node-set), $[A_{ij} - P_{ij}]$ is the difference of the actual ( $A_{ij}$ ) minus the expected ( $P_{ij}$ ) number of edges falling between a particular pair of vertices $i, j \in V$ , and $\delta(g_i, g_j)$ is an indicator (the Kronecker’s) function returning 1 when $g_i = g_j$ .	$Q = \frac{\sum_{i,j} [A_{ij} - P_{ij}] \cdot \delta(g_i, g_j)}{2m}$
Closeness Centrality	$CC$	The inverse of the total binary distance $d(i,j)$ computed on the shortest paths originating from a given node $i \in V$ (where $V$ is the node-set) having destinations all the other nodes $j \in V$ in the network. This measure expresses the node’s reachability from all other nodes in the network.	$CC(i) = \left( \frac{1}{n - 1} \cdot \sum_{j=1, i \neq j}^n d_{ij} \right)^{-1}$
Betweenness Centrality	$CB$	The proportion defined by the number $\sigma(i)$ of the shortest-paths passing through a given node $i$ to the total number $\sigma$ of the network shortest-paths.	$CB(i) = \sigma(i) / \sigma$

\* Sources: [34–36].

A major approach in complex network analysis is the examination of the degree distribution  $p(k)$ , which is defined by the frequency distribution  $(k_i, n(k_i))$  of the unique values  $k_i$  of the node degrees in the network, and is expressed by the relation [19,35]:

$$p(k) = (k_i, n(k_i)), \quad (2)$$

where  $n(k_i)$  is the node frequency (number of nodes) of degree  $k$ . When divided by the total number of nodes  $n(k_i)/n$ , the degree distribution can become a probability distribution [35,37], expressing the probability of meeting a node of degree  $k_i$  in the network. In general, the type of degree distribution can provide insights into the structure and functionality of complex networks, along with some information of the mechanism ruling growth in networks [19,35,38]. Another approach that can provide insights into the network topology is the examination of the sparsity (spy) plot [38] of the graph's adjacency matrix. A spy plot is generally a dot representation of a matrix, displaying nonzero elements with dots. The spy plot can be insightful for pattern recognition in graphs because it suggests a representation of the graph in a matrix space, where connectivity patterns are displayed [38].

#### 2.4. Community Detection Based on Modularity Optimization

In the third step of the methodological framework, the associated visibility graph is divided into connected communities by using the modularity optimization algorithm proposed by the authors of [39]. According to Figure 1c, there are two regions in the phase portrait wherein the trajectories imply that the system is locally unstable but globally stable. As can be observed, the whole system is bi-stable and consists of a pair of attractors of different amplitudes, where two major basins of attraction emerge, implying that the system spends different fractions of its time between them. Provided that this status can reflect the underlying instabilities generating the chaotic oscillations, we apply a community detection analysis based on modularity optimization to evaluate the previous metric observations. In general, the modularity is an objective function expressing the potential of a network to be subdivided into communities [40], as is described in Table 1. The modularity optimization algorithm is a greedy approach dividing a graph into communities according to the criterion of maximizing connectivity within the communities (intra-community connectivity), and consequently of minimizing the connectivity between the communities (inter-community connectivity), as expressed in the relation [40]:

$$\text{maximize } [Q \propto (m_{\text{within communities}} - m_{\text{between communities}})], \quad (3)$$

where  $Q$  is the modularity function and  $m$  is the number of links. The modularity optimization algorithm used in the analysis is applied in two stages [39,40]. At the first, each node in the graph is registered in a separate community. Next, the nodes are step-by-step swept and placed into collective communities, determine by whether the assignment of a node in such a community increases the gain in the weighted modularity function ( $Q_w$ ) of the initial graph. At the second stage, the collective communities are replaced by super-nodes, and the procedure is repeated until the modularity function cannot increase any more [38,40]. For a thorough review of modularity optimization and community detection in graphs, the reader is referred to the review article of [40].

In general, community detection in graphs is a research field that enjoys plenty of applications in network science [36,40], but is unprecedented in time-series analysis. A prime conceptualization of this approach can be found in the work of [31], who divided the Greek COVID-19 infection curve into five connected communities based on modularity optimization, an approach which was projected onto the time-series body and sufficed to predict the prime saturation stage of the pandemic in Greece. Another application appears in the work of [41], who built on the previous community detection of the Greek COVID-19 infection curve to define the knot-vector for the spline regression model's construction. The complex network-defined spline model provided the most accurate predictions amongst a set of available spline and other parametric-fitting models, thus highlighting the potential of community detection (based on modularity optimization) in the time-series analysis to become

a fertile approach in the fields of noise reduction, removing past data, and forecasting. Bearing in mind that it suggests a promising approach for time-series analysis, community detection (based on modularity optimization) is applied to the available voltage oscillations of the TlInTe<sub>2</sub> time-series to detect communities in the time-series body that are considered as relevant due to their high connectivity in the associated visibility graph. Such an approach is expected to reveal parts (communities) in the time-series body that are of major and minor structural importance for the evolution of the TlInTe<sub>2</sub>'s voltage oscillation phenomenon.

### 3. Results and Discussion

The results of computing the network measures of the visibility graph associated with the available voltage oscillation time-series are shown in Table 2. As can be observed, the associated visibility graph is a connective (i.e., including one component) medium-sized graph consisting of 2672 nodes and 11,066 edges (links). The associated visibility graph is a sparse (not dense) graph, including 0.3% of the possible links that can be developed for the certain number of nodes. The degree of the network nodes ranges within the interval [2,324], with an average degree of 8.283 connections. In terms of accessibility, the average path length of the associated visibility graph is 4.496, implying that, on average, two random nodes are distant to each other by almost 4.5 steps of separation. This value is relatively larger than the expected  $\ln n / \ln(\ln n) \stackrel{n=2,672}{\approx} 3.82$  average path length described for scale-free networks, which have a “good” hierarchical structure [19,38] and according to [42] are considered as “ultra-small”. This slight deviation from “scale-freeness”, as expressed by the average path length  $|4.496 - 3.82|/3.82 \approx 17.8\%$ , indicates the existence of (relatively loose) spatial constraints [36], which are obviously related to the chain structure of the source time-series. Further, the network diameter of the visibility graph is 11, expressing that the most distant nodes in the network are a distance of 11 steps of separation away.

**Table 2.** Results of the network measures of the visibility graph associated to the available voltage oscillation time-series of TlInTe<sub>2</sub> (see Figure 1).

Network Measure	Symbol	Value
Network nodes	$n$	2672
Network edges	$m$	11,066
Network components	$\alpha$	1
Graph density	$\rho$	0.003
Maximum degree	$k_{\max}$	324
Minimum degree	$k_{\min}$	2
Average degree	$\langle k \rangle$	8.283
Average path length	$\langle l \rangle$	4.496
Network diameter	$d(G)$	11
Clustering coefficient	$C$	0.772
Modularity	$Q$	0.753
Number of communities	$\text{card}\{g_i\}$	68

Next, the clustering coefficient of the associated visibility graph is 0.772, expressing that a randomly chosen node in the network is 77.2% more likely to have connected neighbors. This value implies a good level of circulation in the information spreading in the network. Finally, the modularity function of the visibility graph is 0.753, implying a good (at the 75% level) tendency of the graph to be divided into communities. In particular, the visibility graph can be divided into 68 communities, which will be further discussed in a following paragraph.

In terms of pattern recognition, Figure 3 shows the degree distribution of the visibility graph associated with the available voltage oscillation time-series of TlInTe<sub>2</sub>, at the metric and log–log scale. As can be observed, the degree distribution fits closely to a power-law pattern ( $R^2 = 0.9608$ ), which is an indication of scale-freeness according to the definition of the scale-free property [19,35].

However, the power-law exponent of the visibility graph  $\gamma_{vis} = -1.222$  does not lie within the typical scale-free range of [2,4] that describes empirical cases of scale-free networks, a fact that may be related to the effect of spatial constraints observed based on the magnitude of the accessibility network measures (average path length, network diameter) and describes the restriction of the visibility graph in developing distant connections. To get a more detailed picture, power-law fittings with cut-offs (see [43]) are also applied to the available degree distribution. As can be observed in Figure 3b,c, the region between degrees  $k = 4$  and  $k = 44$  (including 90.23% of the total data) yields the best possible power-law fitting (adjusted  $R^2 = 0.9765$ ) to the degree-distribution data, and lies within the typical range of scale-freeness describing empirical cases of real-world networks.

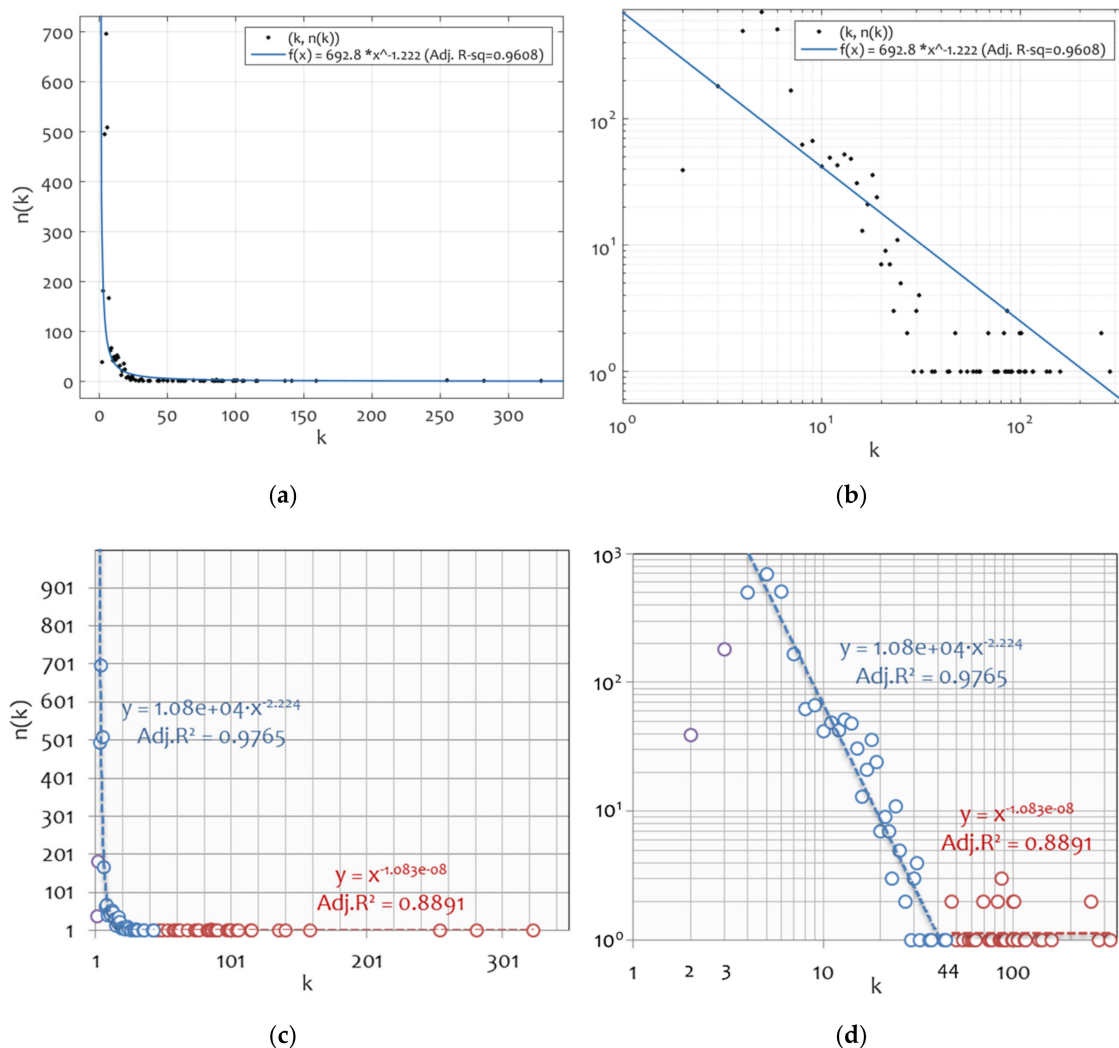


**Figure 3.** The degree distribution of the visibility graph associated to the available voltage oscillation time-series of TlInTe<sub>2</sub> (see Figure 1), shown at (a) metric scale, (b) log-log scale, (c) metric scale with fitting cut-offs at  $k = 3$  and  $k = 44$ , and (d) log-log scale with fitting cut-offs at  $k = 3$ .

On the other hand, the degree distribution in the region of higher degrees (i.e.,  $k > 44$ , including 1.53% of the data), which can be considered the hubs' region, configures a tail that is almost described by a linear and particularly constant pattern (of the form  $y \approx x^{-0} = x^0 = 1$ ). This implies that the main body (90.23% of the data) of the TlInTe<sub>2</sub> voltage oscillation visibility graph is satisfactorily described by the scale-free property, a fact that illustrates the chaotic configuration of the TlInTe<sub>2</sub> voltage oscillation time-series within the context of the fact that the visibility algorithm relates the scale-free property with the fractal-like structure of the time-series [24]. However, the hub

region does not seem to exhibit this scale-free property because its degree distribution is described by linearity (constancy). This observation implies that the hub configuration of the TlInTe<sub>2</sub> voltage oscillation visibility graph does not adhere to the “good” structure of hierarchy expressed by the scale-free property, but instead to a constant rule diverting the hierarchical order. Provided that the hubs in this visibility network are greater in number than those expected by a scale-free pattern, the constant configuration of the hub region can imply the effect of spatial constraints to the extent that the network’s ineffectiveness in developing more distant connections leads to the emergence of more hubs.

Furthermore, Figure 4 shows the spy plot and the Force-Atlas graph layout produced using the open-source software of [44]. Both these diagrams suggest different visualizations of the network topology, with the first illustrating the network embedded in a matrix space and the second in a topological space. In particular, a spy plot is a dot representation of the network’s adjacency matrix, displaying nonzero elements (which express network links) with dots. The spy plot can be insightful for pattern recognition in graphs because it can display connectivity patterns within the adjacency matrix [38]. On the other hand, the Force-Atlas layout is a 2-dimensional representation provided by the open-source software of [44] that is generated by a force-directed algorithm (see [38,45]) with default parameters. The algorithm applies repulsion strengths between network hubs, while it arranges the hubs’ connections into surrounding clusters. Therefore, the graphs that are shown in this layout have their hubs placed at the center of the plane, but at mutually distant positions, so that their distance can be as great as possible, whereas lower-degree nodes are placed as close as possible to their hubs. Provided that both these layouts represent the network embedded in different spaces (i.e., a matrix and force-directed topological space, respectively), they both illustrate different pictures of network topology in a certain growth timeframe. Within this context, the prediction of network growth based on these layouts is linked to pattern recognition, which is made evident by these layouts, namely to the extent that a certain network topology is theoretically or empirically related to a certain growth process (e.g., a lattice-like topology is related to “linear” network growth, revealing the effect of spatial constraints, a random topology is linked to an irregular growth, and the scale-freeness is connected to the “preferential attachment” growth mechanism). For more details see the suggested literature [19,36,38,45].

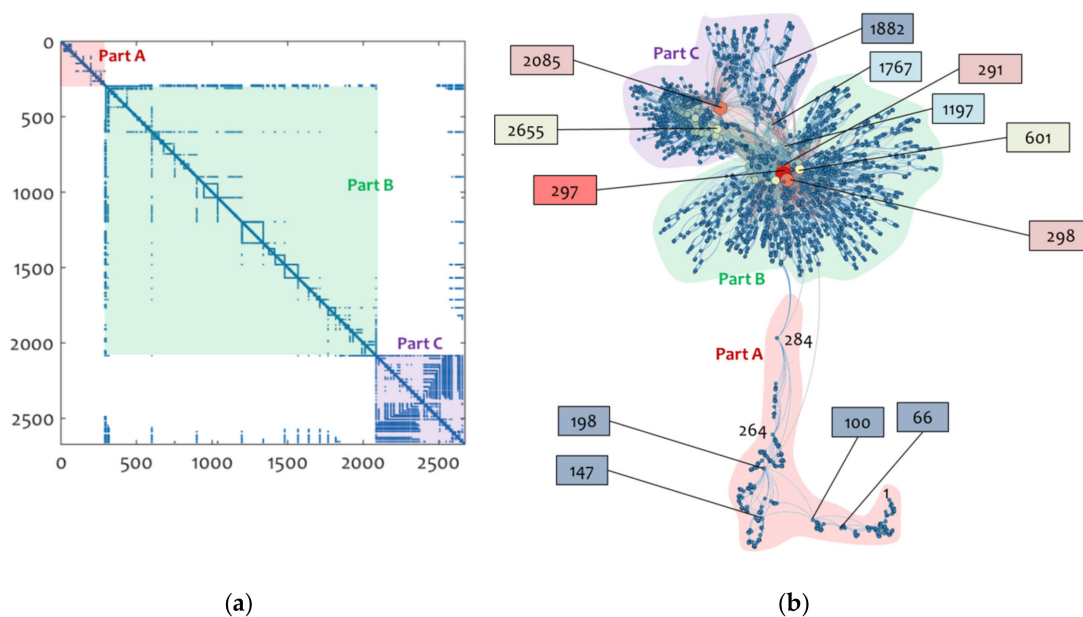


**Figure 4.** (a) Sparsity (spy) plot (see [38]) and (b) the Force-Atlas graph layout [44] of the visibility graph associated to the available voltage oscillation time-series of TlInTe<sub>2</sub> (see Figure 1).

In Figure 4, first, the spy plot illustrates a major arrangement of connections along the main diagonal, which refers to a typical pattern of lattice-like network topologies [38,45]. However, the node region 291–298, along with the node places 601 and 2085, denote some significant connectivity zones in the spy plot, indicating the existence of hubs in the network, which implies that the topology of the visibility graph is more complex than a lattice-like one since it is equipped with hierarchical structures related to the scale-free property, as is captured in the previous degree distribution analysis. Further, the node zones 291–2085 (Figure 4a, Part B) and 2085–2672 (Figure 4a, Part C) illustrate two major square connectivity patterns in the spy plot of the visibility graph, which may correspond to the pair of attractors that are captured in the chaos detection analysis provided by [7] and are shown in Figure 1. An intuitive picture of the chaotic structure of the voltage oscillation time-series of TlInTe<sub>2</sub> can be shaped by observing the fractal-like tiling configured within these square connectivity areas (Figure 4a, Parts B and C).

Next, the network layout of the visibility graph shown in Figure 4 shows a pattern supporting that of the spy plot. Within this context, the Force-Atlas layout of the visibility graph depicts the two major sub-networks defined by the hub families {291,298,297,601,1197} and {2085,2655}, which correspond to Part B (Figure 4b) and Part C (Figure 4b), respectively. This observation adheres to the previous findings of the spy plot examination, and it further supports the linkage between the pair of sub-networks corresponding to Parts B and C (Figure 4b) and the pair-wise structure of attractors extracted in the analysis of [7]. On the other hand, the tail that was observed in the graph and that includes the hub-like nodes {66,147,198,264,284} corresponds to Part A of the spy plot shown in Figure 4a. Overall, the sequential arrangement of Parts A, B, and C, which is observed in both the spy plot and the Force-Atlas layout of Figure 4, illustrates that the visibility network's main constraint is in developing distance connections (a condition that is usually expressed as the "spatial constraints" of the network structure, see [36]), and therefore it supports the finding that the visibility graph associated to TlInTe<sub>2</sub>'s voltage oscillations time-series is described by lattice-like characteristics that can be related to the semi-periodic sections of the time-series.

In the final step of network analysis, a set of secondary time-series is created from the visibility graph. These secondary time-series include network measures that are computed for each node of the visibility graph and are arranged into the node ordering of the source (TlInTe<sub>2</sub>) time-series. In terms of interpretation, each secondary time-series expresses the score that a node of the source time-series has in its associated visibility graph, for a certain measure. Within this context, the secondary time-series that are computed refer to the network measures of degree, clustering coefficient, betweenness and closeness centrality and eccentricity (i.e., the distance of a node to the center of the network, see [35]), and they are shown in Figure 5.

The line diagrams shown in Figure 5a,b illustrate the time-series node ordering of the connectivity hubs in the visibility graph, and are insightful in discriminating the hub families composed of nodes {291,298,297,601} and {2085,2655}, which were previously observed. The two next diagrams of clustering coefficient (Figure 5c) and betweenness centrality (Figure 5d) are perhaps not so insightful in terms of zone detection, but through a careful consideration, they seem to support the central roles of the nodes 291, 298, 297, 601, 2085, and 2655. A cleared picture of the hub-grouping is offered by the diagrams of closeness centrality (Figure 5e) and eccentricity (Figure 5f). However, a clearer observation about these diagrams regards their fractal-like tiling structure, which complies with the chaotic behavior of the voltage oscillation time-series of TlInTe<sub>2</sub>. This observation can configure the research hypothesis that the accessibility-defined measures of the visibility graph can preserve the chaotic characteristics of the source time-series, suggesting a topic of further research.

In the final step of analysis, the associated visibility graph is divided into connected communities by using the modularity optimization algorithm of [39]. The analysis results in 68 communities, as is shown in Table 2 and (in more detail) in Figure 6. As can be observed in Figure 6a, the majority of communities include successive nodes, except from the cases of community Q<sub>4</sub> (Figure 6b) and Q<sub>60</sub> (Figure 6c), which are the two major communities, each containing over 14% of the total time-series

nodes. In particular, community  $Q_4$  includes 388 nodes that are placed in positions from 291 to 2661, and community  $Q_{60}$  includes 403 nodes that are placed in positions from 2085 to 2655. In terms of physical interpretation, the structure of community  $Q_4$  is indicative of the voltage decay that describes the total behavior of the available voltage oscillation time-series of  $\text{TlInTe}_2$ , whereas the structure of community  $Q_5$  includes the characteristic voltage sink recorded in the timeframe from 100 up to 138 s (Figure 1).

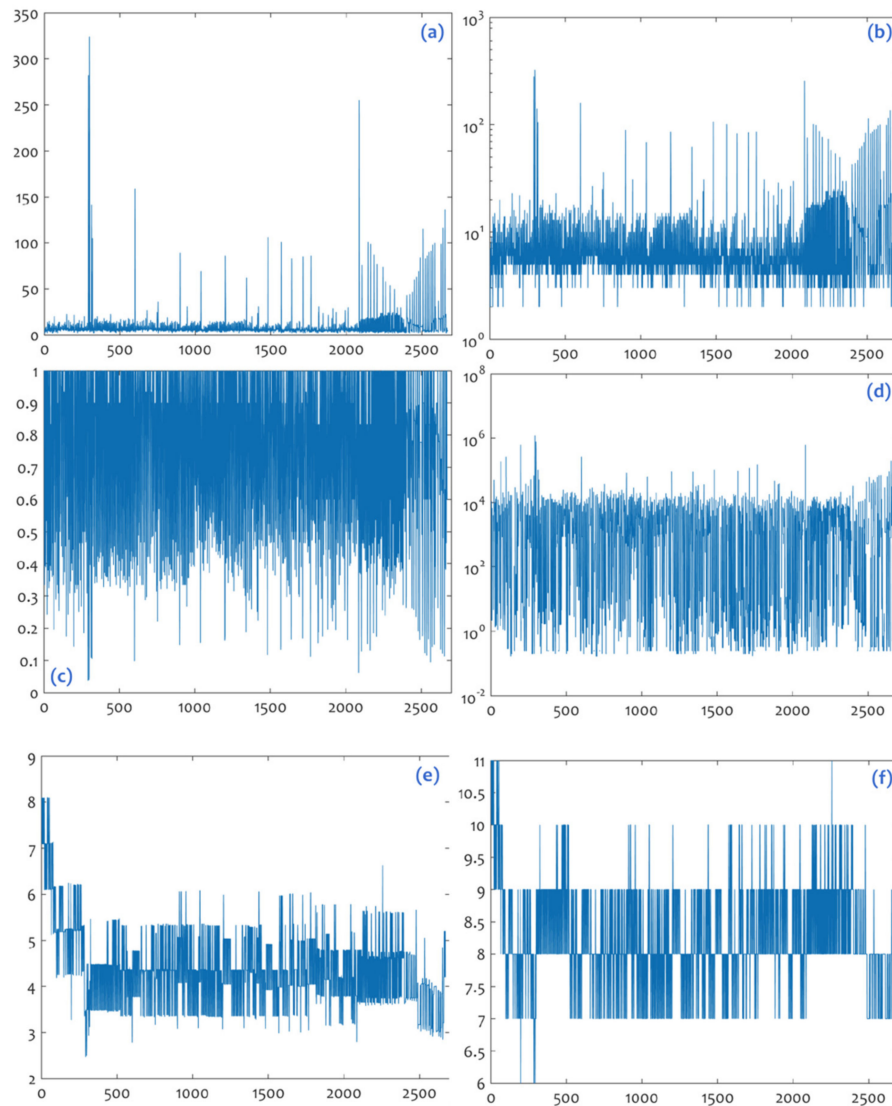


**Figure 5.** Secondary time-series of the network measures of (a) degree (at metric scale), (b) degree (at semi-log scale), (c) clustering coefficient, (d) betweenness centrality (at semi-log scale), (e) closeness centrality, and (f) eccentricity (at semi-log scale), which are computed on the visibility graph associated to the available voltage oscillation time-series of  $\text{TlInTe}_2$  (see Figure 1) and are ordered according to the source ( $\text{TlInTe}_2$ ) time-series ordering.

According to Figure 6d, the majority of communities include individually less than 2% of the total time-series nodes, and only 12 out of 68 communities, namely  $Q_1$  (3.74%),  $Q_2$  (4.19%),  $Q_3$  (2.92%),  $Q_4$  (14.52%),  $Q_5$  (4.08%),  $Q_{11}$  (2.77%),  $Q_{15}$  (2.10%),  $Q_{38}$  (4.42%),  $Q_{52}$  (3.26%),  $Q_{53}$  (3.22%),  $Q_{54}$  (2.99%), and  $Q_{60}$  (15.08%), include over 2% of the total time-series nodes. As already mentioned, 66 out of 68 communities consist of successive (i.e., of the form  $t_k, t_{k+1}$ , where  $k$  is a positive integer) nodes, except from cases  $Q_4$  and  $Q_{60}$ , which also include intermediate gaps. The positioning and the major successive configuration of the communities composing the available voltage oscillation time-series

of  $\text{TlInTe}_2$  imply that this time-series is majorly described by spatial constraints, which are captured by the lattice-like node arrangement along the main diagonal in the spy plot, as well as by the tailed node arrangement shown in the Force-Atlas layout in Figure 4. However, the emergence of two major communities in the visibility graph that exceed the typical sequential structure describing all other communities is related to parts of superior structural behavior in the time-series. This case of unconventional communities complies with the scale-freeness detected in the network analysis shown in Figures 3 and 4, with the chaotic behavior of the source time-series ( $\text{TlInTe}_2$ ) that is the default research hypothesis for this paper, according to the work of [7].

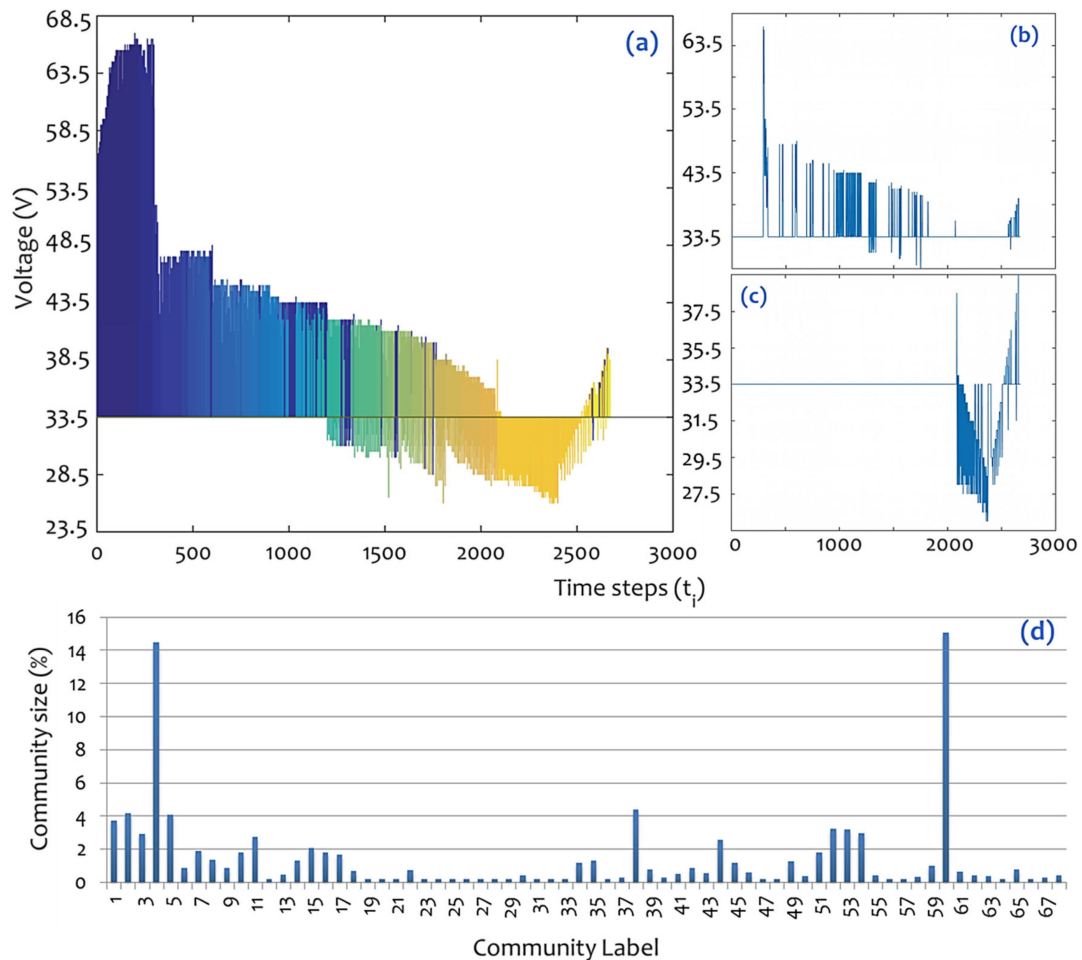


**Figure 6.** Results of the community detection analysis based on the modularity optimization algorithm of Blondel et al. (2008), where (a) is a heat-plot of the community number corresponding to each node in the source ( $\text{TlInTe}_2$ ) time-series, (b) shows the first major community ( $Q_4$ ) containing 14.52% of the total time-series nodes, (c) shows the second major community ( $Q_{60}$ ) containing 15.08% of the total time-series nodes, and (d) is a frequency bar-chart showing the size of each community (% of the total time-series nodes).

The pair-wise structure expressed by the division of the source time-series into a pair of major communities  $Q_4$  and  $Q_{60}$  can also be supported by the examination of the voltage values within the 68 available communities. In particular, Figure 7 shows an arrangement of the box-plots expressing the voltage value distributions within each community, ordered according to the community labeling. As can be observed, there are two areas exceeding the interquartile range of the box-plot distribution of the available communities in Figure 7. These areas include non-typical voltage values of the voltage oscillation time-series of  $\text{TlInTe}_2$ , to the extent that these values exceed 50% of the cases around the mean and lie at the edges (in a two-tailed configuration) of the voltage distribution of  $\text{TlInTe}_2$ .

This result also complies with the previous findings, and can further support the chaotic structure expressed by the pair of attractors configured in the phase portrait of voltage oscillations that is shown in Figure 1.

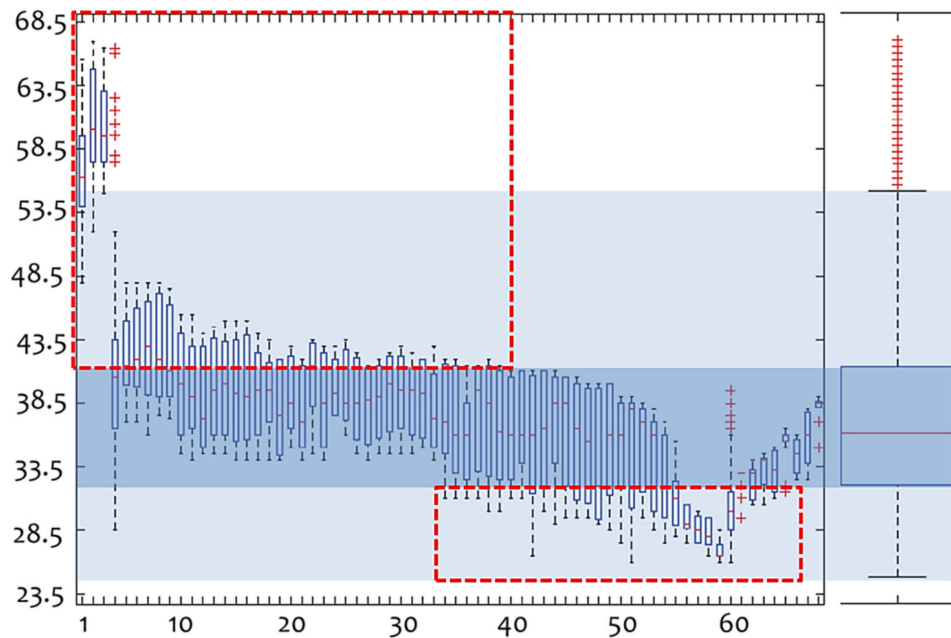


**Figure 7.** Areas exceeding the interquartile range of the box-plot distributions of the 68 communities resulting from the community detection analysis based on the modularity optimization algorithm of [39].

#### 4. Conclusions

This paper proposed a method for examining chaotic structures in semiconductor or alloy voltage oscillation time-series, and studied the case of the thallium indium ditelluride single crystal (TlInTe<sub>2</sub>) semiconductor, which was by default described by quasi-periodic and chaotic self-excited voltage oscillations. This approach was expected to reveal information about the transport phenomena, which are related to the current filaments and their connections, and to contribute to the understanding of this phenomenon as ruled by an electrothermal mechanism. The analysis built on the complex network analysis of time-series, and applied the visibility graph algorithm of [24], which is established in the literature for its ability to convert fractal series into scale-free networks, to transform the available time-series into a complex network, and to study the topological properties of the visibility graph instead of those of the source time-series. The results showed that the main body of the visibility graph is described by a good structure of hierarchy that illustrates the already known chaotic structure of the TlInTe<sub>2</sub> voltage oscillations' time-series. However, the network analysis also revealed a lattice-like configuration of the visibility graph that is related to the network's inability to develop distant connections, and is consistent to the general chain-like structure of the source time-series. The lattice-like characteristics captured by the analysis can be related to semi-periodic sections of the time-series. Furthermore, the community detection analysis revealed a pair of major communities that can relate to the pair-wise attractor of the TlInTe<sub>2</sub> voltage oscillation time-series' phase portrait, a fact which further supports the link between the scale-freeness of the visibility graph and the chaotic structure of the source time-series. Furthermore, the network analysis revealed that the accessibility network measures (closeness centrality and eccentricity) of the visibility graph are better representatives of the chaotic properties of the source time-series than the measures of degree, clustering, and betweenness centrality. Overall, the analysis detected that the hybrid chaotic and quasi-periodic structure of the source time-series is converted to a hybrid scale-free and lattice like

topology in the associated visibility graph, a fact that promotes the synthetic approach in statistical physics and the complex network analysis of time-series as a method dealing with the complexity of semiconductor and alloy physics.

**Author Contributions:** Conceptualization, D.T., L.M. and M.P.H.; methodology, D.T. and M.P.H.; software, D.T. and M.P.H.; validation, D.T., L.M. and M.P.H.; formal analysis, D.T. and M.P.H.; investigation, L.M. and M.P.H.; resources, L.M. and M.P.H.; data curation, D.T., L.M. and M.P.H.; writing—original draft preparation D.T. and M.P.H.; writing—review and editing, D.T., L.M. and M.P.H.; visualization, D.T. and M.P.H.; supervision, L.M.; project administration, L.M.; funding acquisition, n/a. All authors have read and agreed to the published version of the manuscript.

**Funding:** This research received no external funding.

**Conflicts of Interest:** The authors declare no conflict of interest.

## References

- Girard, P. Electrostatic force microscopy: Principles and some applications to semiconductors. *Nanotechnology* **2001**, *12*, 485. [[CrossRef](#)]
- Yu, P.Y.; Cardona, M. *Fundamentals of Semiconductors. Physics and Materials Properties*; Springer: Berlin/Heidelberg, Germany, 2005. [[CrossRef](#)]
- McKelvey, J.P. *Solid State and Semiconductor Physics*; Harper & Row: Manhattan, NY, USA, 2018.
- Dugdale, J.S. *The Electrical Properties of Metals and Alloys*; Courier Dover Publications: Mineola, NY, USA, 2016.
- Peinke, J.; Parisi, J.; Rossler, O.E.; Stoop, R. *Encounter with Chaos: Self-organized Hierarchical Complexity in Semiconductor Experiments*; Springer Science & Business Media: Berlin, Germany, 2012.
- Hanias, M.P.; Anagnostopoulos, A.N. Negative-differential-resistance effects in the TlGaTe<sub>2</sub> ternary semiconductor. *Phys. Rev. B* **1993**, *47*, 4261. [[CrossRef](#)] [[PubMed](#)]
- Hanias, M.P.; Kalomiro, J.A.; Karakotsou, C.; Anagnostopoulos, A.N.; Spyridelis, J. Quasiperiodic and chaotic self-excited voltage oscillations in TlInTe<sub>2</sub>. *Phys. Rev. B* **1994**, *49*, 16994–16998. [[CrossRef](#)] [[PubMed](#)]
- Panich, A.M. Electronic properties and phase transitions in low-dimensional semiconductors. *J. Phys. Condens. Matter* **2008**, *20*, 293202. [[CrossRef](#)]
- Godzhaev, E.M.; Gyu'lmamedov, K.D.; Allakhyarov, E.A. Current–voltage characteristics of TlInX<sub>2</sub>–TlSmX<sub>2</sub> (X= S, Se, Te) alloys. *Inorg. Mater.* **2003**, *39*, 113–116. [[CrossRef](#)]
- Abay, B.; Gurbulak, B.; Yildirim, M.; Efeoglu, H.; Yogurtcu, Y.K. Electrothermal investigation of the switching phenomena in p-type TlInSe<sub>2</sub> single crystals. *Phys. Status Solidi* **1996**, *153*, 145–151. [[CrossRef](#)]
- Miller, A.; Miller, D.A.; Smith, S.D. Dynamic non-linear optical processes in semiconductors. *Adv. Phys.* **1981**, *30*, 697–800. [[CrossRef](#)]
- Bonilla, L.L.; Grahm, H.T. Non-linear dynamics of semiconductor superlattices. *Rep. Prog. Phys.* **2005**, *68*, 577. [[CrossRef](#)]
- Shore, K.A. Non-linear dynamics and chaos in semiconductor laser devices. *Solid-State Electron.* **1987**, *30*, 59–65. [[CrossRef](#)]
- Ahrenkiel, R.K.; Keyes, B.M.; Dunlavy, D.J. Non-linear recombination processes in photovoltaic semiconductors. *Sol. Cells* **1991**, *30*, 163–176. [[CrossRef](#)]
- King, J.R.; Meere, M.G.; Rogers, T.G. Asymptotic analysis of a non-linear model for substitutional diffusion in semiconductors. *Z. Angew. Math. Phys.* **1992**, *43*, 505–525. [[CrossRef](#)]
- Kumar, S.; Kumar, P.R. Queueing network models in the design and analysis of semiconductor wafer fabs. *IEEE Trans. Robot. Autom.* **2001**, *17*, 548–561. [[CrossRef](#)]
- Zhang, L.; Pan, W.; Yan, L.; Luo, B.; Zou, X.; Xu, M. Cluster synchronization of coupled semiconductor lasers network with complex topology. *IEEE J. Sel. Top. Quantum Electron.* **2019**, *25*, 1–7. [[CrossRef](#)]
- Brandes, U.; Robins, G.; McCranie, A.; Wasserman, S. What is network science? *Netw. Sci.* **2013**, *1*, 1–15. [[CrossRef](#)]
- Barabasi, A.L. *Network Science*; Cambridge University Press: Cambridge, UK, 2016.
- Gao, Z.-K.; Yang, Y.-X.; Fang, P.-C.; Zou, Y.; Xia, C.-Y.; Du, M. Multiscale complex network analysis for analyzing experimental multivariate time-series. *Europhys. Lett.* **2015**, *109*, 30005. [[CrossRef](#)]
- Zhang, J.; Small, M. Complex network from pseudoperiodic time-series: Topology versus dynamics. *Phys. Rev. Lett.* **2006**, *96*, 238701. [[CrossRef](#)]

22. Yang, Y.; Yang, H. Complex network-based time-series analysis. *Phys. A: Stat. Mech. Appl.* **2008**, *387*, 1381–1386. [[CrossRef](#)]
23. Xu, X.; Zhang, J.; Small, M. Superfamily phenomena and motifs of networks induced from time-series. *Proc. Natl. Acad. Sci. USA* **2008**, *105*, 19601–19605. [[CrossRef](#)]
24. Lacasa, L.; Luque, B.; Ballesteros, F.; Luque, J.; Nuno, J.C. From time-series to complex networks: The visibility graph. *Proc. Natl. Acad. Sci. USA* **2008**, *105*, 4972–4975. [[CrossRef](#)]
25. Luque, B.; Lacasa, L.; Ballesteros, F.; Luque, J. Horizontal visibility graphs: Exact results for random time-series. *Phys. Rev. E* **2009**, *80*, 046103. [[CrossRef](#)]
26. Liu, C.; Zhou, W.X.; Yuan, W.K. Statistical properties of visibility graph of energy dissipation rates in three-dimensional fully developed turbulence. *Physica A* **2010**, *389*, 2675–2681. [[CrossRef](#)]
27. Charakopoulos, A.K.; Karakasidis, T.E.; Papanicolaou, P.N.; Liakopoulos, A. The application of complex network time-series analysis in turbulent heated jets. *Chaos* **2014**, *24*, 024408. [[CrossRef](#)]
28. Gao, Z.K.; Cai, Q.; Yang, Y.X.; Dang, W.D.; Zhang, S.S. Multiscale limited penetrable horizontal visibility graph for analyzing nonlinear time-series. *Sci. Rep.* **2016**, *6*, 35622. [[CrossRef](#)]
29. Jiang, W.; Wei, B.; Zhan, J.; Xie, C.; Zhou, D. A visibility graph power averaging aggregation operator: A methodology based on network analysis. *Comput. Ind. Eng.* **2016**, *101*, 260–268. [[CrossRef](#)]
30. Iacobello, G.; Scarsoglio, S.; Ridolfi, L. Visibility graph analysis of wall turbulence time-series. *Phys. Lett. A* **2017**, *382*, 1–11. [[CrossRef](#)]
31. Tsiotas, D.; Magafas, L. The effect of anti-COVID-19 policies on the evolution of the disease: A complex network analysis of the successful case of Greece. *Physics* **2020**, *2*, 325–339. [[CrossRef](#)]
32. Tsiotas, D.; Charakopoulos, A. Visibility in the topology of complex networks: Introducing a new approach. *Phys. A: Stat. Mech. Appl.* **2018**, *505*, 280–292. [[CrossRef](#)]
33. Tsiotas, D.; Charakopoulos, A. VisExpA: Visibility expansion algorithm in the topology of complex networks. *SoftwareX* **2020**, *11*, 100379. [[CrossRef](#)]
34. Koschutzki, D.; Lehmann, K.; Peeters, L.; Richter, S. Centrality indices. In *Network Analysis*; Brandes, U., Erlebach, T., Eds.; Springer: Berlin/Heidelberg, Germany, 2005; pp. 16–61.
35. Newman, M.E.J. *Networks: An Introduction*; Oxford University Press: Oxford, UK, 2010. [[CrossRef](#)]
36. Barthelemy, M. Spatial networks. *Phys. Rep.* **2011**, *499*, 1–101. [[CrossRef](#)]
37. Walpole, R.E.; Myers, R.H.; Myers, S.L.; Ye, K. *Probability & Statistics for Engineers & Scientists*; Prentice Hall Publications: New York, NY, USA, 2012.
38. Tsiotas, D. Detecting different topologies immanent in scalefree networks with the same degree distribution. *Proc. Natl. Acad. Sci. USA* **2019**, *116*, 6701–6706. [[CrossRef](#)]
39. Blondel, V.; Guillaume, J.-L.; Lambiotte, R.; Lefebvre, E. Fast unfolding of communities in large networks. *J. Stat. Mech.* **2008**, *10*, P10008. [[CrossRef](#)]
40. Fortunato, S. Community detection in graphs. *Phys. Rep.* **2010**, *486*, 75–174. [[CrossRef](#)]
41. Demertzis, K.; Tsiotas, D.; Magafas, L. Modeling and forecasting the COVID-19 temporal spread in Greece: An exploratory approach based on complex network defined splines. *Int. J. Environ. Res. Public Health* **2020**, *17*, 4693. [[CrossRef](#)] [[PubMed](#)]
42. Cohen, R.; Havlin, S. Scale-Free Networks are Ultrasmall. *Phys. Rev. Lett.* **2003**, *90*, 058701. [[CrossRef](#)]
43. Clauset, A.; Shalizi, C.R.; Newmann, M.E. Power-law distributions in empirical data. *SIAM Rev.* **2009**, *51*, 661–703. [[CrossRef](#)]
44. Bastian, M.; Heymann, S.; Jacomy, M. Gephi: An open source software for exploring and manipulating networks. In *Proceedings of the Third International ICWSM Conference, San Jose, CA, USA, 17–20 May 2009*; pp. 361–362.
45. Tsiotas, D. Detecting differences in the topology of scale-free networks grown under time-dynamic topological fitness. *Sci. Rep.* **2020**, *10*, 10630. [[CrossRef](#)]

**Publisher’s Note:** MDPI stays neutral with regard to jurisdictional claims in published maps and institutional affiliations.



© 2020 by the authors. Licensee MDPI, Basel, Switzerland. This article is an open access article distributed under the terms and conditions of the Creative Commons Attribution (CC BY) license (<http://creativecommons.org/licenses/by/4.0/>).